Modulation of $A\beta_{42}$ Fibrillation in the Presence of Vitamin A Metabolite: Insights from Molecular Dynamics Simulations

A

Dissertation submitted

in partial fulfilment of the requirements for the degree of

Master of Science

in

Chemistry

By

Vibhuti Gupta

(Reg. No. 302202011)

Under the guidance of

Dr. Bhupesh Goyal

DEPARTMENT OF CHEMISTRY AND BIOCHEMISTRY

THAPAR INSTITUTE OF ENGINEERING AND TECHNOLOGY, PATIALA

147004

JULY 31, 2024

DECLARATION

I hereby declare that the dissertation entitled **Modulation of $A\beta_{42}$ Fibrillation in the Presence of Vitamin A Metabolite: Insights from Molecular Dynamics Simulations** presented in partial fulfilment of the requirements for the award of the degree of **Master of Science in Chemistry** to **Department of Chemistry and Biochemistry, Thapar Institute of Engineering and Technology, Patiala** is a record of the independent research conducted by me from January to July 2024 under the guidance of Dr. Bhupesh Goyal. Additionally, none of the components of this dissertation have been submitted to another university for consideration of a different degree or diploma.

Signature of Candidate

Date: 31th July, 2024 Vibhuti Gupta

Place: TIET, Patiala Regn. No. 302202011

CERTIFICATE

This is to certify that the dissertation entitled **Modulation of $A\beta_{42}$ Fibrillation in the Presence of Vitamin A Metabolite: Insights from Molecular Dynamics Simulations** being submitted by **Ms. Vibhuti Gupta** to **Department of Chemistry and Biochemistry, Thapar Institute of Engineering and Technology, Patiala** in partial fulfilment of the requirements for the award of the degree of **Master of Science in Chemistry**, is an authentic record of the work carried out by the candidate under my/our guidance and supervision. She has fulfilled the requirements for the submission of this dissertation, which to my knowledge has reached the requisite standard. The results embodied in the dissertation have not been submitted in part or full to any other University or Institute for the award of any other degree or diploma.

Date: 31th July, 2024

Place: TIET, Patiala

Bhupesh Goyal

Signature

Dr. Bhupesh Goyal

Associate Professor

Department of Chemistry and Biochemistry

ACKNOWLEDGEMENT

First and foremost, I express my heartfelt gratitude to Almighty God for his countless blessings, knowledge, and opportunities, which have enabled me to successfully complete my dissertation. I am deeply thankful to Dr. Manmohan Chhibber, Professor and Head of the Department of Chemistry and Biochemistry, for giving me the opportunity to delve into the world of research through this dissertation.

I extend my sincere thanks to my supervisor, Dr. Bhupesh Goyal, for his outstanding guidance, expertise, and unwavering support throughout the research process. His insights and suggestions have been crucial in shaping this thesis, and I am profoundly grateful for his mentorship.

I am immensely thankful to my mentor, Ms. Arushi, who guided me and monitored my entire project work. Her instruction in research methodologies and her constant support have been invaluable. Furthermore, I am very grateful to the research scholars in my lab Ms. Diksha, Ms. Tanishka, Ms. Anisha, Ms. Gurmeet, and Mr. Ishwar, for their inspiring guidance and cooperation during this research work.

My deepest thanks go to the Thapar Institute of Engineering and Technology (TIET) for providing the necessary facilities and infrastructure for this study.

In conclusion, the completion of this thesis is the result of collaborative efforts and support of an exceptional network of individuals, for which I am genuinely thankful.

Thank you all.
Date: 31th July, 2024
Place: TIET, Patiala

Vibhuti Gupta

ABSTRACT

Alzheimer's disease (AD) is a neurodegenerative disorder characterized by misfolding and consequent aggregation of amyloid-β (Aβ) protein, resulting in the formation of amyloid plaques within the brain. The best possible therapy approach for AD treatment is to prevent Aβ aggregation. Joshi et al. evaluated 18 fat-soluble and water-soluble vitamins and reported vitamin A metabolite (retinoic acid) significantly inhibited $A\beta_{42}$ aggregation. Thioflavin T (ThT) fluorescence analysis depicted a concentration-dependent decrease in both the primary and secondary nucleation process of $A\beta_{42}$ on the inclusion of retinoic acid. Moreover, dynamic light scattering (DLS) analysis did not depict the presence of large assemblies for retinoic acid alone. Co-incubation of $A\beta_{42}$ oligomer with retinoic acid notably increased the cell viability to 97 ± 6% highlighting reduction of cytotoxicity of $A\beta_{42}$ oligomers by retinoic acid. Besides extensive experimental research, the molecular interactions and binding mechanism behind the inhibitory potential of retinoic acid on $A\beta_{42}$ aggregation is still unknown. Thus, computational techniques to investigate the molecular mechanism in which retinoic acid blocks self-fibrillation of $A\beta_{42}$ aggregation were performed. The molecular docking result highlighted favourable binding of retinoic acid with $A\beta_{42}$ monomer having binding energy −6.10 kcal mol^{-1}. The RMSD and RMSF analyses depicted reduced conformational fluctuations in $A\beta_{42}$ monomer on the addition of retinoic acid. Notably, an increase in helix content was observed in the $A\beta_{42}$ monomer from 44.80 ± 2.20 to 54.40 ± 0.88% which depicted reduced aggregation propensity of $A\beta_{42}$ monomer in the presence of retinoic acid. Moreover, the average number of intramolecular hydrogen bonds was increased from 19.10 ± 0.96 to 21.07 ± 1.05 on the incorporation of retinoic acid, which confirms the increase in the helical conformation of $A\beta_{42}$ monomer. PCA, FEL, and conformational clustering analyses depicted enhanced conformational homogeneity of $A\beta_{42}$ monomer-retinoic acid complex. The binding free energy analysis ($\Delta G_{binding}$ = –54.89 ± 14.07 kJ mol^{-1}) indicated favourable binding of retinoic acid with $A\beta_{42}$ monomer. Additionally, binding of central hydrophobic core (CHC) residues Leu17 (–5.95 kJ mol^{-1}), Phe20 (–6.19 kJ mol^{-1}), and Ala21 (–3.53 kJ mol^{-1}) of $A\beta_{42}$ monomer to retinoic acid highlighted the lower aggregation tendency of $A\beta_{42}$ monomer. The molecular insights into binding interactions of retinoic acid to $A\beta_{42}$ peptide will be beneficial for designing new potent inhibitors as a therapeutic approach against AD.

TABLE OF CONTENTS

LIST OF TABLES

LIST OF FIGURES

LIST OF ABBREVIATIONS

Abbreviations	Full meaning/name
AD	Alzheimer's Disease
PD	Parkinson's Disease
ALS	Amylotrophic Lateral Sclerosis
Aβ	Amyloid–beta
APP	Amyloid Precursor Protein
BBB	Blood-Brain Barrier
ThT	Thioflavin T
DLS	Dynamic Light Scattering
TEM	Transmission Electron Microscopy
MD	Molecular Dynamics
AChE	Acetylcholinesterase
PDB	Protein Data Bank
AFM	Atomic Force Microscopy
C	Catechin
EC	Epicatechin
ECG	Epicatechin Gallate
EGC	Epigallocatechin
EGCG	Epigallocatechin Gallate
CHC	Central Hydrophobic Core
RMSD	Root Mean Square Deviation
RMSF	Root Mean Square Fluctuation
R_g	Radius of gyration
SASA	Solvent Accessible Surface Area
DSSP	Dictionary of Secondary Structure of Proteins
MM–PBSA	Molecular Mechanics Poisson Boltzmann Surface Area
GA	Gallic Acid
TA	Tannic Acid
EA	Ellagic Acid
GEN	Genistein
SA	Syringic Acid
MeG	Methyl Gallate
REMD	Replica Exchange Molecular Dynamics
GBP	Gabapentin
FDA	Food and Drug Administration
NT	N–terminal
CDP	Cyclic dipeptide
CD	Circular Dichroism
RCSB	Research Collaboratory for Structural Bioinformatics
HF	Hartree Fock
ATB	Automated Topology Builder
LGA	Lamarckian Genetic Algorithm
PCA	Principal Component Analysis
FEL	Free Energy Landscape
PC	Principal Component

CHAPTER 1: Introduction

Proteins are polymers made up of amino acids that form an integral part of the biological system, assisting in building cytoskeleton, enzymes, muscles, and hormones.[1] The native structure of proteins is a mature, three-dimensional form that governs the proper functioning of life processes involving proteins.[2,3] However, protein misfolding arises from any abnormal deviation from the normal protein folding process which consequently results in various neurodegenerative disorders associated with this aberrant folding, including Alzheimer's disease (AD), amyotrophic lateral sclerosis (ALS), Huntington's disease (HD), and Parkinson's disease (PD). [4,5] According to World Alzheimer report, 2024, dementia affects more than 55 million people globally, with AD being the most common cause and this number is expected to rise to 139 million by 2050.[6] The estimated annual cost for treatment of AD is about US $1.3 trillion. Symptoms of AD include impairment of memory, cognitive function, physical ability, and psychosis.[7,8]

The primary cause of AD pathology involves the accumulation of senile plaques[9] and neurofibrillary tangles.[10] Senile plaques are composed of aggregates of amyloid-β (Aβ) peptide, which consist of 39 to 43 amino acid residues[11]. Formation of Aβ peptide is initiated by proteolytic cleavage of a transmembrane precursor protein known as amyloid precursor protein (APP) by the β–and γ–secretase enzymes.[12] Aβ exists in two alloforms $A\beta_{40}$, and $A\beta_{42}$, with the latter being a more aggregation-prone and neurotoxic variant.[13] In a healthy human brain, $A\beta_{40}$ and $A\beta_{42}$ peptides are present in monomeric form, however, in brain tissues of AD patients, the Aβ peptide undergoes a conformational change into aggregation-prone β–sheets, forming insoluble oligomeric and fibrillar aggregates which further transforms into neuritic plaques.[14]

Various inhibitors that restrict the aggregation of Aβ peptide or disintegrate preformed fibrillar Aβ aggregates serve as prospective therapeutic candidates for AD treatment. The inhibitors include small molecules,[15] peptides,[16] and nanoparticles,[17] which inhibit aggregation by various strategies such as blocking the expression of APP, restricting cleavage of APP, inhibiting aggregation of Aβ monomer, and disrupting the preformed aggregates.[18,19] Small molecule inhibitors are advantageous over other inhibitors due to blood-brain barrier (BBB) permeability, immunologically tolerant behaviour, and stability in biological fluids and tissues.[20] Several studies have indicated that vitamins, including vitamin –E (tocopherol),[21] D (calciferol),[22] K (phylloquinone),[23] C (ascorbic acid),[24] and B12 (cyanocobalamine)[25] as potent inhibitors of $A\beta_{42}$ aggregation which can delay the onset of dementia.

Joshi et al. tested various vitamin metabolites and discovered that vitamin A metabolite (retinoic acid) induced a robust effect on $A\beta_{42}$ aggregation.[26] Thioflavin T (ThT) fluorescence assay highlighted retinoic acid block $A\beta_{42}$ aggregation by decreasing both primary and secondary nucleation processes in a dose-dependent manner. The results revealed that retinoic acid inhibited aggregation of $A\beta_{42}$, while vitamin E, in its self-assembled (micellar) state, accelerated the same but inhibited it when present in its soluble monomeric form. Additionally, ThT-based aggregation assay containing a mixture of vitamin A and E metabolites at a concentration range of 0.15–0.25 molar equivalent vitamin E, and 0–7 molar equivalent vitamin A, cancelled the net effect of both vitamins on aggregation of $A\beta_{42}$ monomer. TEM images displayed a reduction of $A\beta_{42}$ fibrils on co-incubation with retinoic acid (2:20 μM). Furthermore, the effect of retinoic acid on $A\beta_{42}$ aggregation in an *in vivo* system using the *Caenorhabditis elegans* model, it was observed that retinoic acid decreased $A\beta_{42}$ aggregation resulting in increased overall fitness of the worms. Cytotoxic profile depicted that $A\beta_{42}$ oligomers reduced the viability of SH-SY5Y cells to 66 ± 2% which was notably increased to 97 ± 6 % in the presence of retinoic acid (5 molar equivalent). Despite extensive research, the binding mechanism behind inhibitory capability of retinoic acid against $A\beta_{42}$ remains unclear. To explore the mechanism of action behind the inhibition of $A\beta_{42}$ monomer aggregation by retinoic acid, as well as to understand the interactions between them, computational analyses have been performed.

Table 1. Small molecule inhibitors of $A\beta_{42}$ aggregation.

S.No.	Small molecule	Key findings	References
1.	Berberine	• Molecular mechanism of berberine inhibiting $A\beta_{16-21}$ aggregation was investigated using computational techniques. • RMSD, RMSF, and R_g analyses depicted higher structural stability and compactness of $A\beta_{16-21}$ (PDB ID: 1Z0Q) in the presence of berberine. • The α- helix increased from 0.02 to 0.54% and β–sheet content reduced from 32.80 to 1.36%, indicating a reduced aggregation propensity of $A\beta_{16-21}$ in the presence of berberine. • Berberine hindered the oligomerization process of $A\beta_{16-21}$ by forming a stable complex with $A\beta_{16-21}$.	Qais et al.[27]
2.	Anthocyanidins [cyanidin, malvidin, delphinidin, peonidin, pelargonidin, and petunidin]	• Inhibitory mechanisms of anthocyanidins on $A\beta_{1-42}$ peptide were investigated using MD simulations. • Cyanidin (CYA), malvidin (MAL), and peonidin (PEO) displayed binding in the N–terminal, C–terminal and central polar region of $A\beta_{42}$ monomer (PDB ID: 1Z0Q). • The three anthocyanidins increased helix content and reduced coil and β–sheet formation in $A\beta_{42}$ monomer, depicting a reduced tendency of $A\beta_{42}$ monomer to aggregate. • Intramolecular hydrogen bonds in $A\beta_{42}$-CYA complex, $A\beta_{42}$-MAL, and $A\beta_{42}$-PEO were found to be 23.451, 25.658, and 26.410, respectively. • Salt bridge analysis revealed significant prevention of salt bridge formation by increasing the distance between Asp23–Lys28 residues to 1.17nm, 1.08nm, and 0.90 nm in presence of CYA, MAL, and PEO, respectively. • CYA, MAL, and PEO effectively inhibited $A\beta_{42}$ aggregation.	Zakaria et al.[28]
3.	Benzothiazole-piperazine small hybrid molecule (compound **1**)	• Benzothiazole-piperazine (compound **1**) was found to be a potent multi-target-directed ligand against AD inhibiting both AChE and $A\beta_{1-42}$ monomer. • RMSF and SASA analyses revealed an increase in conformational stability of $A\beta_{1-42}$ monomer	Mishra et al.[29]

		(PDB ID: 1IYT) in the presence of compound **1**. • It exhibited binding free energy –16.10 ± 0.18 kcal mol^{-1} with $A\beta_{1-42}$ monomer. • Compound **1** displayed good inhibitory activity of 80.70% (IC_{50} = 44.64 μM) against $A\beta_{1-42}$ monomer in comparison to curcumin (50.23%) taken as reference in the ThT assay. • Confocal laser scanning microscopy indicated a decrease in fluorescence intensity and TEM images illustrated fewer aggregates of $A\beta_{1-42}$ in the presence of compound **1** indicating the ability to inhibit $A\beta_{1-42}$ aggregation. • Compound **1** depicted neuroprotective ability by increasing the cell viability in dose-dependent manner against H_2O_2-mediated SH-SY5Y and Neuro2A cells. • Compound **1** improved spatial memory in the scopolamine-mediated mice model. • The studies displayed that compound **1** can prove to be a potent therapeutic agent for AD treatment.	
4.	Neferine	• Regulatory impact of Neferine on $A\beta_{42}$ and tau K18 aggregation was investigated. • From molecular docking, it was found that neferine displayed a binding energy of –8.39 kcal mol^{-1} with $A\beta_{42}$ monomer (PDB ID: 1Z0Q). • ThT fluorescence assay revealed that neferine (25 μM) decreased the fluorescence intensity and inhibited $A\beta_{42}$ aggregation and disaggregation. • Atomic force microscopy (AFM) images depicted a reduction in particle length in $A\beta_{42}$ incubated with neferine. • MD simulation results indicated that neferine induced a conformational shift from β-sheet to α-helix leading to disruption of $A\beta_{42}$ aggregation. • Neferine (25 μM) indicated a neuroprotective effect against $A\beta_{42}$ induced neurotoxicity by increasing the cell viability in HT22 mouse hippocampal neuronal cells. • Nefereine is a promising therapeutic for AD.	Nam et al.[30]
5.	Catechins [catechin(C), epicatechin (EC),	• The binding interaction of the five catechins present in green tea with $A\beta_{42}$ monomer was investigated using the ensemble docking method.	Firouzi et al.[31]

	epicatechin gallate (ECG), epigallocatechin (EGC), epigallocatechin gallate(EGCG)]	• Molecular docking results depicted that all the catechins interacted with a maximum number of aromatic residues in the region Tyr10 to Phe20 of $A\beta_{42}$ monomer including the CHC region. • The binding interaction was favoured through formation of hydrogen bonds between EGCG and EGC with $A\beta_{42}$ monomer in comparison with C, EC, and ECG. • However, all the catechins, particularly EGCG inhibited $A\beta_{42}$ aggregation.	
6.	Natural polyphenols [gallic acid (GA), epigallocatechin gallate (EGCG), tannic acid (TA), ellagic acid (EA), genistein (GEN), syringic acid (SA), methyl gallate (MeG), 4-hydroxyfavone (4-HF), and 2-hydroxyfavone (2-HF)]	• The dual-therapeutic effects of natural polyphenols against ferroptosis and AD were investigated through molecular docking and *in-vitro* techniques. • Molecular docking revealed the highest binding free energy of tannic acid (TA), reported as –38 kJ mol^{-1} with $A\beta_{42}$ monomer (PDB ID: 1Z0Q). • ThT fluorescence assay displayed 82% $A\beta_{42}$ aggregation inhibition at 1:5 ($A\beta_{42}$: TA) molar ratio. • MTT assay depicted that TA and EGCG increased the cell viability to 63 and 69%, respectively at 20 µM when compared to $A\beta_{42}$ alone (34.8%). • Overall, TA effectively inhibited the $A\beta_{42}$ aggregation.	Baruah et al.[32]
7.	Four flavonoids (1-4) derived from Psoralea Fructus	• *In silico* technique was employed to discover the effect of natural small molecules isolated from Psoralea Fructus on $A\beta_{42}$ aggregation. • Molecular docking of 1-4 compounds with $A\beta_{42}$ monomer (PDB ID: 1Z0Q) revealed docking scores of −5.23, −4.78, −4.27, and −4.00 kcal mol^{-1}, respectively. • RMSF analysis revealed lower fluctuations highlighting enhanced stability of $A\beta_{42}$ monomer in presence of compounds 1-4. • The four compounds (1-4) displayed strong binding energy ($\Delta G_{binding}$) of –23.45, –19.04, –15.34, and –14.08 kcal mol^{-1} respectively, with $A\beta_{42}$ monomer. • The residues His14, Gln15, Val18, Phe19, and Glu22 of $A\beta_{42}$ monomer were involved in strong binding with the four flavonoids depicting their anti-aggregation properties.	Radwan et al.[33]

8.	EGCG and genistein	• The mechanistic insights into inhibitory mechanisms of EGCG and genistein against $A\beta_{42}$ monomer were investigated using computational techniques. • From molecular docking, the binding energy of EGCG was noted to be −4.28 kcal mol^{-1} and of genistein was found to be −5.10 kcal mol^{-1} with $A\beta_{42}$ monomer (PDB ID: 1IYT). • RMSD, R_g, RMSF, and SASA data collectively indicated that EGCG and genistein inhibit conformational changes in $A\beta_{42}$ monomer. • The EGCG and genistein reduced the β–sheet content of $A\beta_{42}$ monomer from 2.75 ± 1.82 to 0% with a concomitant increase in random coil from 24.69 ± 4.58 to 28.00 ± 8.02% in the presence of genistein and 29.52 ± 8.90% in presence of EGCG. • Increase in helix content of $A\beta_{42}$ monomer was observed in presence of genistein from 45.28 ± 2.42 to 43.76 ± 12.85%, however, EGCG displayed less pronounced effect on helical content of $A\beta_{42}$ monomer. • MM-PBSA analysis highlighted favourable binding of EGCG with the CHC region of $A\beta_{42}$ monomer with $\Delta G_{binding}$ = –20.06 ± 4.62 kcal mol^{-1}, while the $\Delta G_{binding}$ of genistein was observed to be −3.59 ± 0.78 kcal mol^{-1}. • Therefore, EGCG was found to be promising inhibitor in self-fibrillation of $A\beta_{42}$ monomer.	Fang et al.[34]
9.	1-benzylamino-2-hydroxyalkyl derivatives (24 compounds)	• Using *in silico*, *in vivo* and *in vitro* techniques, the dual inhibitory effects of 1-benzylamino-2-hydroxyalkyl derivatives on Aβ and tau aggregation were analyzed. • Thioflavin S (ThS) fluorescence assay in recombinant *Escherichia coli* cells depicted that compound 18 displayed 80.00% $A\beta_{42}$ inhibition and 68.30% tau inhibition, at a molar ratio 1:1 (10 μM). • MD simulation results depicted enhanced stability of $A\beta_{42}$ monomer (PDB ID: 1IYT) by an increase in its helical content in presence of compound 18. • Molecular docking result revealed notable effect of chirality of compound 18 on anti-aggregation of $A\beta_{42}$ monomer and tau. The *S*-isomer was observed to have a strong inhibitory effect on $A\beta_{42}$ aggregation while *R*-isomer was noted to be a better inhibitor of tau aggregation.	Pasieka et al.[35]

		• Kinetic studies using ThT assay depicted that compound 18 kinetically inhibited $A\beta_{40}$ aggregation by 41% at 10 μM concentration (1:1), by a decrease in nucleation and elongation of $A\beta_{40}$ monomer in presence of compound 18. • Compound 18 proved to be a potential inhibitor of Aβ aggregation.	
10.	Gabapentin (GBP)	• Inhibitory potential of the FDA-approved compound gabapentin (GBP) was investigated using *in silico* and *in vitro* methods. • A docking score of −3.402 and binding energy (ΔG_{bind}) of −25.2 kcal mol^{-1} was noted for $A\beta_{42}$-GBP complex. • The secondary structure analysis revealed that the helix content increased to 13.8 ± 2.7 from 10.8 ± 1.6% and β–sheet content reduced to 6.8 ± 1.8 from 13.3 ± 2.7% in $A\beta_{42}$ monomer (PDB ID: 1IYT) on incorporation of GBP. • Fluorescence displayed an increase in the peak intensity of tyrosine fluorescence at 304 nm with the addition of GBP (250 μM), which highlights the presence of molecular interactions between GBP and $A\beta_{42}$ peptide. • From the absorbance assay, a reduction in the absorbance spectra of $A\beta_{42}$ was observed in the presence of GBP in a concentration-dependent manner, which depicted reduced aggregation of $A\beta_{42}$ in the presence of GBP. • AFM images indicated a reduction in $A\beta_{42}$ aggregates in the presence of GBP. • GBP effectively inhibited the $A\beta_{42}$ aggregation.	González-Sanmiguel et al.[36]
11.	2-Octahydroisoquinolin-2(1H)-ylethanamine (M-30)	• *In silico*, *in vitro*, and *in vivo* assays were employed to identify the neuroprotective properties of 2-Octahydroisoquinolin-2(1H)-ylethanamine (M-30). • M-30 displayed a docking score of –6.096 and interacted with the C–terminal portion of $A\beta_{42}$ monomer (PDB ID: 1IYT). • Furthermore, MD simulations study depicted that M-30 reduced the β–sheet content of $A\beta_{42}$ monomer from ~10.22 to 7.03%. • Circular dichroism (CD) experiments also revealed a reduction in β–sheet content of $A\beta_{42}$ monomer (32 μM) in the presence of M30 (160 μM). • From the MTT assay, IC_{50} value of M30 was observed to be 680 ± 9 nM.	Peters et al.[37]

- *In vivo* assay in wild-type mice revealed an increase in spatial memory in the hippocampus of mice in the presence of M30.
- M-30 proved to be a promising inhibitor against $A\beta_{42}$ aggregation.

Table 2. Peptide-based inhibitors against $A\beta_{42}$ aggregation.

S.No.	Peptide/ peptidomimetics	Key findings	References
1.	14 hydrophobic peptides (NT-01 to NT-14)	• *In vitro* and *in silico* techniques were employed to hydrophobic peptides designed by single mutation at Val18 in the $A\beta_{42}$ fragment (KLVFFAE) with leucine and proline. • NT-02, NT-03, and NT-13 displayed 57.61, 54.26, and 48.41% inhibition against $A\beta_{42}$ aggregation as observed from the ThT assay. • MTT assay depicted cell viability of 94.30, 92.41, and 92.16% in the presence of NT-02, NT-03, and NT-13. • TEM images revealed complete abolishment of $A\beta_{42}$ aggregates on incubation with NT-02, NT-03, and NT-13 peptides, therefore, preventing the formation of higher order fibrillary $A\beta_{42}$ aggregates. • Molecular docking results revealed that NT-02, NT-03, and NT-13 peptides have selective binding interactions with N–terminal residues of $A\beta_{42}$ monomer (PDB ID: 1Z0Q) thus decreasing the propensity of $A\beta_{42}$ aggregation.	Mallesh et al.[38]
2.	Peptide C1, C2, P1-P14	• Peptides, C1, C2, and P1-P14 were designed by one/two-point mutation in the amyloidogenic region (Lys16–Ala21) of $A\beta_{42}$ peptide with N–terminal acetylation and C–terminal N–methylation. • The binding strength and effectiveness of peptide inhibitors were investigated against $A\beta_{42}$ monomer (PDB ID: 1IYT) and $A\beta_{42}$ fibril (PDB ID: 2MXU) using computational techniques. • A lower R_g value was observed in $A\beta_{42}$ monomer on the incorporation of P12, which indicates more compactness of $A\beta_{42}$ monomer with P12. Moreover, RMSD and RMSF analysis depicted increased structural stability of $A\beta_{42}$ monomer in the presence of P12. • MM-GBSA results displayed that DKAPFF (P12) demonstrated the highest binding free energy ($\Delta G_{binding}$ = –70.17 kcal mol^{-1}) with $A\beta_{42}$ monomer. • P12 displayed binding in the CHC and C–terminal region of $A\beta_{42}$ monomer.	Kundal et al.[39]

		• P12 displayed effective inhibition against $A\beta_{42}$ aggregation.	
3.	$A\beta_{14-23}$ peptidomimetics (I-V) with cyclic dipeptide units.	• A set of $A\beta_{14-23}$ peptidomimetics with cyclic dipeptide (CDP) units at different positions were synthesized and aggregation behaviour was evaluated using *in vitro* and molecular docking. • The time-dependent ThT fluorescence assay revealed reduced $A\beta_{42}$ aggregation in the following order: peptidomimetic V > II > III. • AFM and TEM images highlighted decreased aggregates of $A\beta_{42}$ monomer in the presence of peptidomimetic V. • Cell viability of 97% was found in cultured neuronal cells (SH-SY5Y), in the presence of peptidomimetic V at 10 µM (1:1). • Peptidomimetic V displayed a binding energy of –5.3 kcal mol^{-1} with $A\beta_{42}$ monomer (PDB ID: 1Z0Q). • Peptidomimetic V significantly inhibited $A\beta_{42}$ aggregation and enhanced the stability of $A\beta_{42}$ monomer.	Konar et al.[40]
4.	Heptapeptide LVFFARK (L-LK7, D-LK7)	• Chiral influence of peptide-based inhibitor LVFFARK (LK7) was investigated using *in vitro* and *in silico* methods. • ThT assay depicted that D-LK7 effectively reduced the fluorescence intensity of $A\beta_{42}$ aggregates in a dose-dependent manner. • D-LK7 rescued the neuronal SH-SY5Y cells by increasing the cell viability in concentration concentration-dependent manner resulting in reduced $A\beta_{42}$-induced cytotoxicity. • CD spectroscopy revealed a reduction in β–sheet content of $A\beta_{42}$ from 47.6 to 20.4% at 48 hour in the presence of D-LK7. • D-LK7 enantiomer displayed a higher binding energy of –4.4 kcal mol^{-1} than L-LK7 (–4.1 kcal mol^{-1}) with $A\beta_{42}$ monomer (PDB ID: 1IYT). • The results highlighted that D-LK7 enantiomer of LVFFARK hexapeptide increased the stability of $A\beta_{42}$ monomer, thus, efficiently inhibiting $A\beta_{42}$ aggregation.	Liu et al.[41]

CHAPTER 3: Computational details

3.1. Protein and ligand preparation

MD simulations were conducted on two distinct systems: $A\beta_{42}$ monomer alone and $A\beta_{42}$ monomer-retinoic acid complex. The $A\beta_{42}$ monomer is $D_1AEFRHDSGY_{10}EVHHQKLVFF_{20}AEDVGSNKGA_{30}IIGLMVGGVV_{40}IA_{42}$. The structure of full length $A\beta_{42}$ monomer (PDB ID: 1Z0Q)[42] was obtained from RCSB protein data bank[43] (Fig. 1a). The 2D chemical structure of retinoic acid was drawn by using ChemDraw Ultra 15.0[44] (Fig. 1b). Afterwards, the structure was optimized by Gaussian09[45] using Hartree-Fock (HF) method employing 6-31G* basis set. The Automated Topology Builder (ATB) server[46] was used to obtain CHARMM36 force field[47] parameters for retinoic acid.

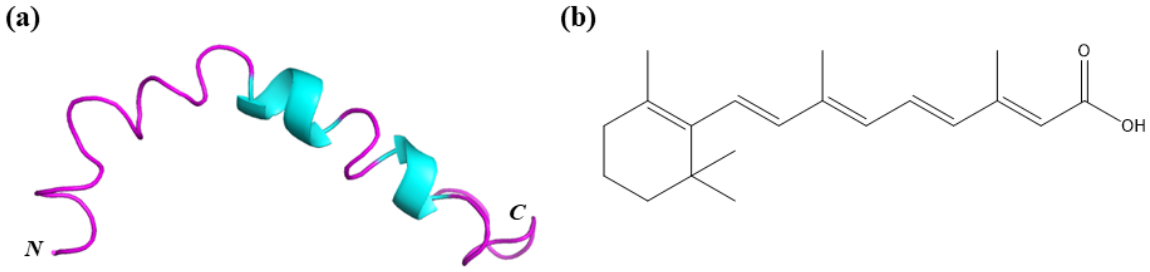

Fig. 1. Structure of $A\beta_{42}$ monomer (PDB ID: 1Z0Q) in panel a; the 2D molecular structure of vitamin A metabolite (retinoic acid) in panel b.

3.2. Molecular docking

Molecular docking was performed to calculate the binding energy and key interactions of retinoic acid with $A\beta_{42}$ monomer using AutoDock Vina software.[48] The PDBQT files were generated using the AutoDock tools.[49] Polar hydrogens and Kollman charges were added to $A\beta_{42}$ monomer. Gasteiger charges were incorporated into $A\beta_{42}$ monomer-retinoic acid system. The $A\beta_{42}$ monomer-retinoic acid was enclosed within a grid box having spacing set to 0.50 Å and grid dimensions were set to 104 Å × 50 Å × 48 Å. The grid center was positioned at x = –2.798, y = 2.195 and z = –8.644. The Lamarckian Genetic Algorithm (LGA)[50] was included in the docking procedure that uses Genetic, Solis & Wets algorithm.[51] The docking results were inspected using LigPlot+[52] and PyMOL software.[53]

3.3. System preparation for MD simulations

The MD simulations were performed using GROMACS software[54] with CHARMM36 force field for $A\beta_{42}$ monomer and $A\beta_{42}$ monomer-retinoic acid systems (Table 3). The systems were positioned in a cubic box[27,28,29,34,36] having dimensions 7.17 × 7.17 × 7.17 nm^3. The systems were solvated with TIP3P water molecules[55] and the number of water molecules was 11717, and 11709 in $A\beta_{42}$ monomer and $A\beta_{42}$ monomer-retinoic acid, respectively. 0.15 M concentration of NaCl was incorporated in the systems to maintain the physiological pH neutrality. Afterwards, the steepest descent minimization algorithm was used for energy minimization and systems were equilibrated using *NVT* and *NPT* for a period of 500 ps at 310 K temperature. For maintaining the temperature of 310 K, V-scaling method[56] was employed and for maintaining the pressure of 1 bar Parrinello-Rahman's method[57] was used. The LINCS algorithm was used to constrain bonds involving hydrogen atoms of $A\beta_{42}$ monomer, while the SETTLE algorithm was applied to constrain bonds within water.[58] The particle Mesh Ewald (PME) method[59] was used to investigate electrostatic interactions. The cut-off value for van der Waals interactions was set to 1 nm. Repeat simulation of $A\beta_{42}$ monomer was also performed using the same method and algorithms, but different initial velocities, to check the reproducibility of MD simulations.

Table 3. Details of MD simulated systems.

System	Simulation time (ns)	Box dimensions (nm)	Number of water molecules in box
$A\beta_{42}$ monomer	100 × 2	7.17 × 7.17 × 7.17	11717
$A\beta_{42}$ monomer-retinoic acid	100 × 1	7.17 × 7.17 × 7.17	11709

3.4. Analyses details

Analyses of generated MD trajectories of the systems were done using GROMACS tools and conformations were visualized using PyMOL software.[53] For calculating root-mean-square deviation (RMSD) the gmx_rms tool was used, through which deviations of the backbone atoms from their original position were evaluated for $A\beta_{42}$ monomer and $A\beta_{42}$ monomer-retinoic acid complex. The gmx_rmsf tool was employed for calculating root-mean-square fluctuations (RMSF) and gmx_sasa tool was used to analyze solvent-accessible surface area (SASA) for sidechain atoms of $A\beta_{42}$ monomer in contact with solvent molecules. The gmx_hbond tool was employed to calculate intramolecular hydrogen bonds present in $A\beta_{42}$ monomer and $A\beta_{42}$ monomer-retinoic acid complex. The dictionary of secondary structure of

proteins (DSSP) was used to calculate secondary structure content using the gmx do_dssp tool.[60] For clustering analysis, Daura et al. algorithm was used by employing the gmx_cluster.[61]

3.5. PCA, FEL, and binding free energy analysis

PCA was done using the gmx_covar tool to analyze conformational fluctuations. FEL was done using the gmx_sham tool. The binding free energy of retinoic acid with $A\beta_{42}$ monomer was calculated using molecular mechanics Poisson-Boltzmann surface area (MM-PBSA) method by employing g_mmpbsa tool.[62]

CHAPTER 4: Results and discussion

4.1. Molecular docking studies and key interactions of retinoic acid with Aβ$_{42}$ monomer

To gain insights into the binding energy and interactions of retinoic acid with Aβ$_{42}$ monomer molecular docking was performed. Retinoic acid displayed a favourable binding energy of –6.10 kcal mol^{-1} with Aβ$_{42}$ monomer (Table 4). Zakaria et al. reported a binding energy of –6.1 kcal mol^{-1} on docking of cyanidin with Aβ$_{42}$ monomer (PDB ID: 1Z0Q), consistent with this result.[28] The oxygen atom of carbonyl group of retinoic acid was involved in hydrogen bond formation (0.22 nm) with main chain hydrogen atom of NH of Val39 residue of Aβ$_{42}$ monomer (Fig. 2a). Peters et al. reported the small molecule 2-Octahydroisoquinolin-2(1H)-ylethanamine (M30) formed hydrogen bond with Val39 and Ala42 of Aβ$_{42}$ monomer (PDB ID: 1IYT).[63] In addition to this, seven residues of Aβ$_{42}$ monomer present in C–terminal region (Asn27, Ala30, Ile31, Met35, Gly38, Ile41, Ala42), formed hydrophobic contacts with retinoic acid as displayed in the 2D interaction map (Fig. 2b). Afterwards, MD simulations were performed to investigate mechanistic insights into the inhibitory potential of retinoic acid against Aβ$_{42}$ aggregation.

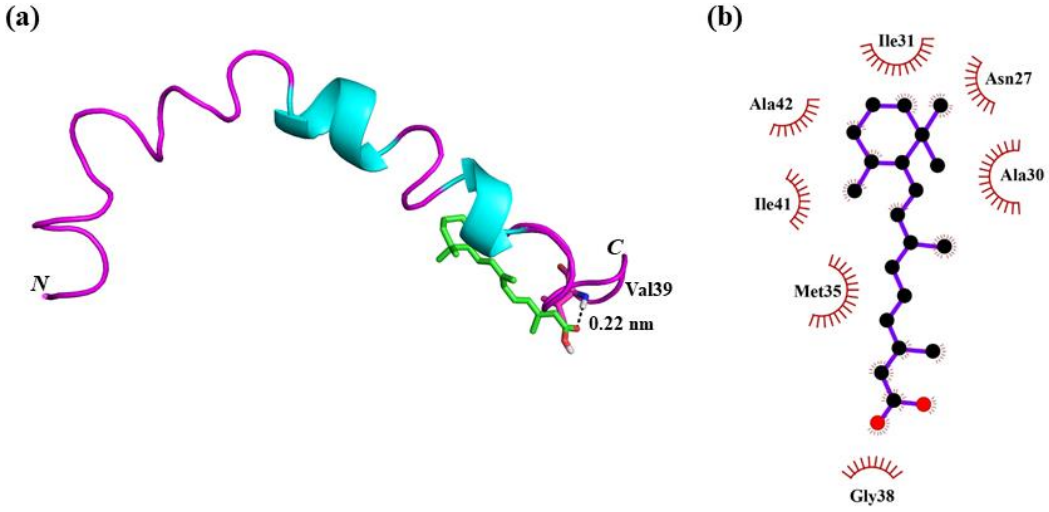

Fig. 2. Docking pose of retinoic acid at the C–terminal region of Aβ$_{42}$ monomer, displaying hydrogen bond in dotted black line (panel a); 2D interaction map showing the hydrophobic contacts in red semicircles between Aβ$_{42}$ monomer residues and retinoic acid (panel b).

Table 4. Details of key interactions of retinoic acid to $A\beta_{42}$ monomer.

Compound	AutoDock Vina binding energy (kcal/mol)	Residue and atoms of $A\beta_{42}$ monomer and retinoic acid involved in hydrogen bond formation			Residues of $A\beta_{42}$ monomer involved in hydrophobic contacts with retinoic acid
		Residue	Atom[a]	Distance (nm)	
Retinoic acid	–6.10	Val39	NH : OC	0.22	Asn27, Ala30, Ile31, Met35, Gly38, Ile41, Ala42

[a]Atom on the left corresponds to $A\beta_{42}$ monomer; whereas on the right corresponds to retinoic acid.

4.2. Impact of retinoic acid on the conformational fluctuations in $A\beta_{42}$ monomer

RMSD and RMSF analyses were performed to investigate the structural stability of $A\beta_{42}$ monomer in the absence and presence of retinoic acid. The average RMSD of $A\beta_{42}$ monomer was noted to be 0.85 ± 0.04 nm (Fig. 3a). On inclusion of retinoic acid, the average RMSD of $A\beta_{42}$ monomer reduced to 0.73 ± 0.04 nm which depicts enhanced structural stability and lesser deviations of $A\beta_{42}$ monomer. The RMSD value of $A\beta_{42}$ monomer is reduced by ~0.12 nm in the presence of retinoic acid. Fang et al. reported a reduction in RMSD of $A\beta_{42}$ monomer on the incorporation of genistein by ~0.14 nm, which is consistent with this study.[34] Furthermore, the repeat simulation of $A\beta_{42}$ monomer displayed the same RMSD pattern as observed for simulation 1 (Fig. 3b) which highlights the reproducibility of MD simulations. Afterward, RMSF analysis was employed to investigate fluctuations of the Cα atoms of $A\beta_{42}$ monomer (Fig. 3c). The RMSF analysis revealed an average RMSF of $A\beta_{42}$ monomer was 0.68 ± 0.03 nm which notably decreased to 0.47 ± 0.02 nm in presence of retinoic acid. The N-terminal, CHC, and C-terminal regions influence $A\beta_{42}$ fibrillation.[64] The fluctuations remarkably decreased for Asp1–His6, Gly9–Ile31, and Gly37–Ala42 residues corresponding to N–terminal, CHC, and C–terminal of $A\beta_{42}$ monomer on incorporation of retinoic acid highlighting reduced aggregation propensity of $A\beta_{42}$ monomer.

4.3. SASA evaluation of Aβ42 monomer and Aβ42 monomer-retinoic acid

SASA analysis was performed to investigate the exposure of Aβ42 monomer to solvent molecules in the presence and absence of retinoic acid (Fig. 3d). The average SASA of Aβ42 monomer in the presence of retinoic acid reduced to 48.82 ± 2.44 nm^2 from 52.91 ± 2.65 nm^2. The SASA value was noted to be the same in both systems until ~35 ns after which it decreased significantly in Aβ42 monomer-retinoic acid complex. The reduced SASA value depicted a lesser exposure of Aβ42 monomer to solvent in the presence of retinoic acid indicating a lesser tendency to aggregate.

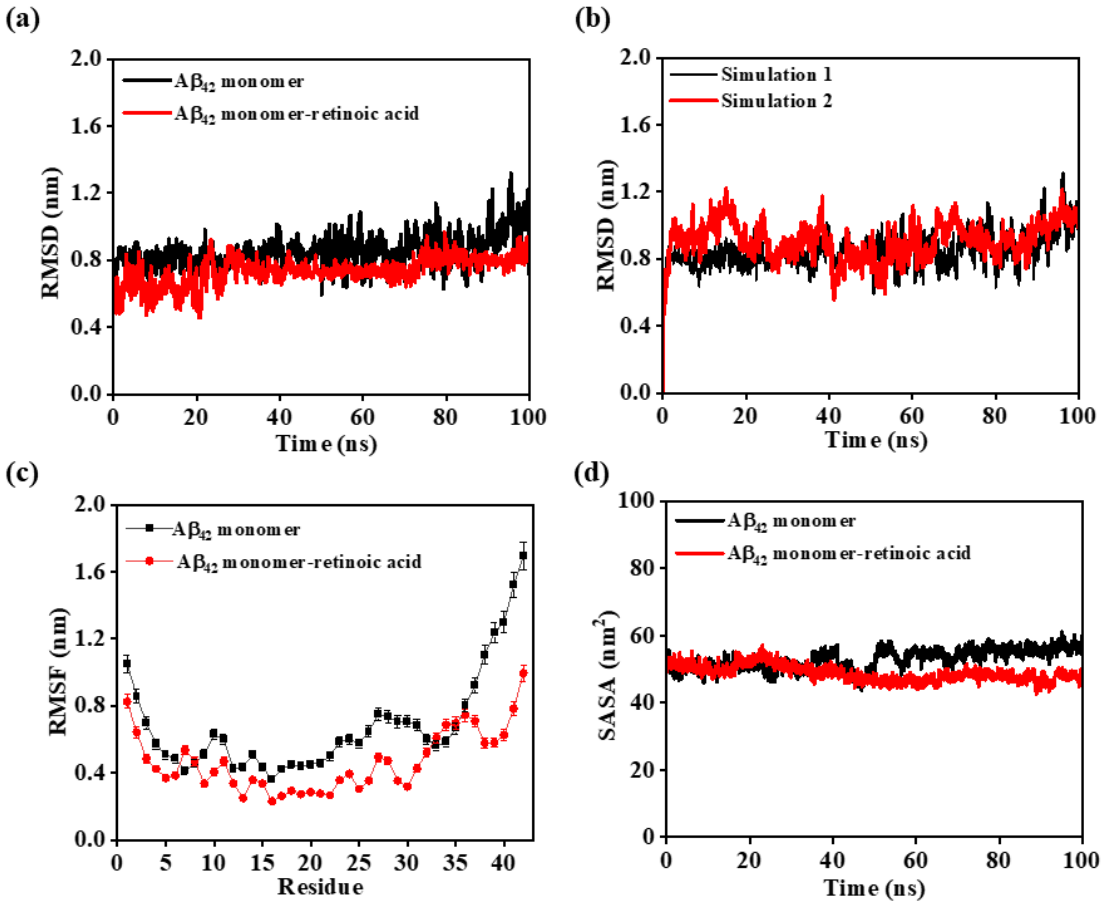

Fig. 3. RMSD for the backbone atoms (panel a); RMSD of repeat simulation of Aβ42 monomer alone (panel b); RMSF calculated for Cα atoms (panel c); SASA for side chain atoms in two systems (panel d).

4.4. Impact of retinoic acid on the Aβ42 monomer conformational ensemble

The colour-coded map of two systems are shown in Fig. 4. The secondary structure contents of Aβ42 monomer was noted to be 44.80 ± 2.20% helix, 0.00 ± 0.00% β−sheet, 38.40 ± 3.65% coil, 11.00 ± 0.98% bend, and 5.80 ± 1.04% turn. In the presence of retinoic acid, the secondary

structure contents of Aβ$_{42}$ monomer were found to have 54.40 ± 0.88% helix, 0.00 ± 0.00% β–sheet, 30.00 ± 1.26% coil, 8.00 ± 0.57% bend, and 7.60 ± 0.46% turn (Table 5). Zakaria et al. reported that Aβ$_{42}$ monomer exhibited 53% helical content when exposed to peonidin, corroborating the results observed in this study.[28] The results depicted a remarkable increase in helix with a simultaneous decrease in coil content of Aβ$_{42}$ monomer in the presence of retinoic acid, highlighting enhanced stability and reduced aggregation tendency of Aβ$_{42}$ monomer.

Table 5. Secondary structure contents in two systems.

Secondary structure content (%)	Aβ$_{42}$ monomer	Aβ$_{42}$ monomer-retinoic acid
Helix[a]	44.80 ± 2.20	54.40 ± 0.88
β–sheet[b]	0.00 ± 0.00	0.00 ± 0.00
Coil	38.40 ± 3.65	30.00 ± 1.26
Bend	11.00 ± 0.98	8.00 ± 0.57
Turn	5.80 ± 1.04	7.60 ± 0.46

[a]Helix = α–helix + π–helix + 3$_{10}$–helix; [b]β–sheet = β–strand + β–bridge

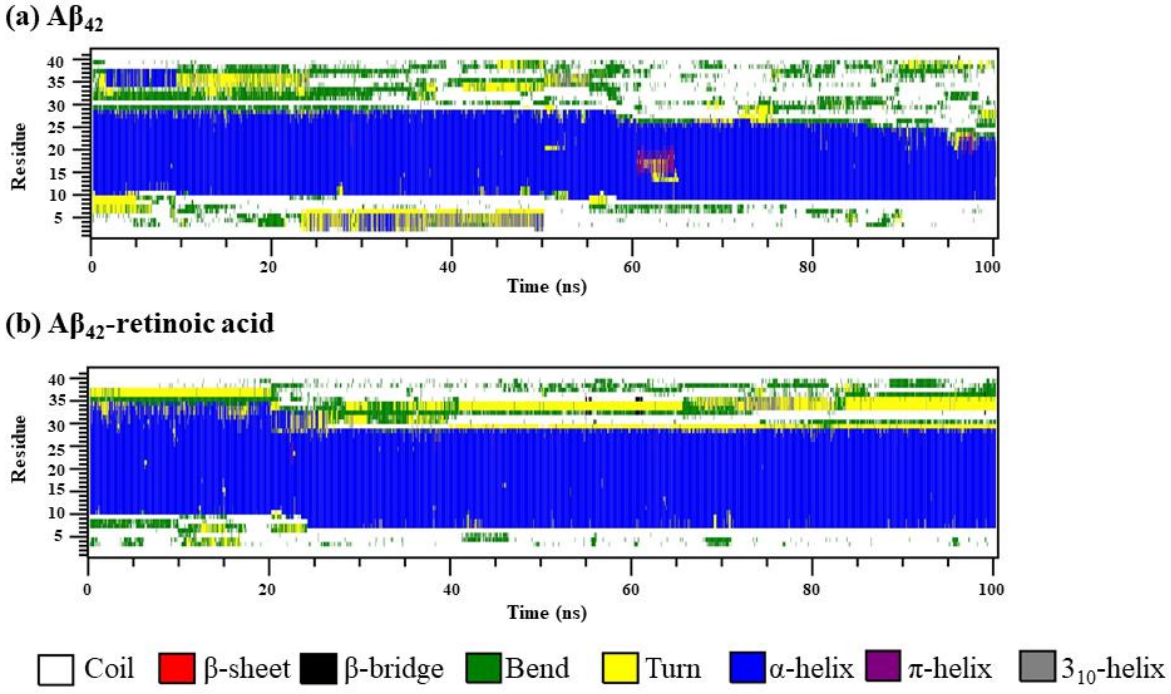

Fig. 4. Colour-coded map of secondary structure content of (a) Aβ$_{42}$ monomer, and (b) Aβ$_{42}$ monomer-retinoic acid complex.

Per-residue secondary structure analysis was performed to calculate the secondary structure content of Aβ$_{42}$ monomer residues in absence and presence of retinoic acid (Fig. 4). The helix content was significantly increased for Asp1–Arg5, Val18–Glu22, and Val24–Lys28 residues with concomitant decrease in coil content for residues Asp1–Arg5, and Val18–Gly29 of Aβ$_{42}$

monomer (Fig. 4a-b). Interestingly, the coil conformation was converted into a helix of $A\beta_{42}$ monomer on the incorporation of retinoic acid. Retinoic acid induced a decrease in bend conformation for Asp1–Ala2, Phe4–Arg5, Val18–Ala21, Asp23–Gly25, Asn27–Lys28, and Ile32–Leu34 of $A\beta_{42}$ monomer (Fig. 4c). However, Glu22–Ile31 residues of $A\beta_{42}$ monomer displayed increase in turn conformation on the addition of retinoic acid (Fig. 4d). From secondary structure analysis, a notable increase in the helix content can be observed in N–terminal and C–terminal region, depicting stability of native helical conformation of $A\beta_{42}$ monomer on the incorporation of retinoic acid.

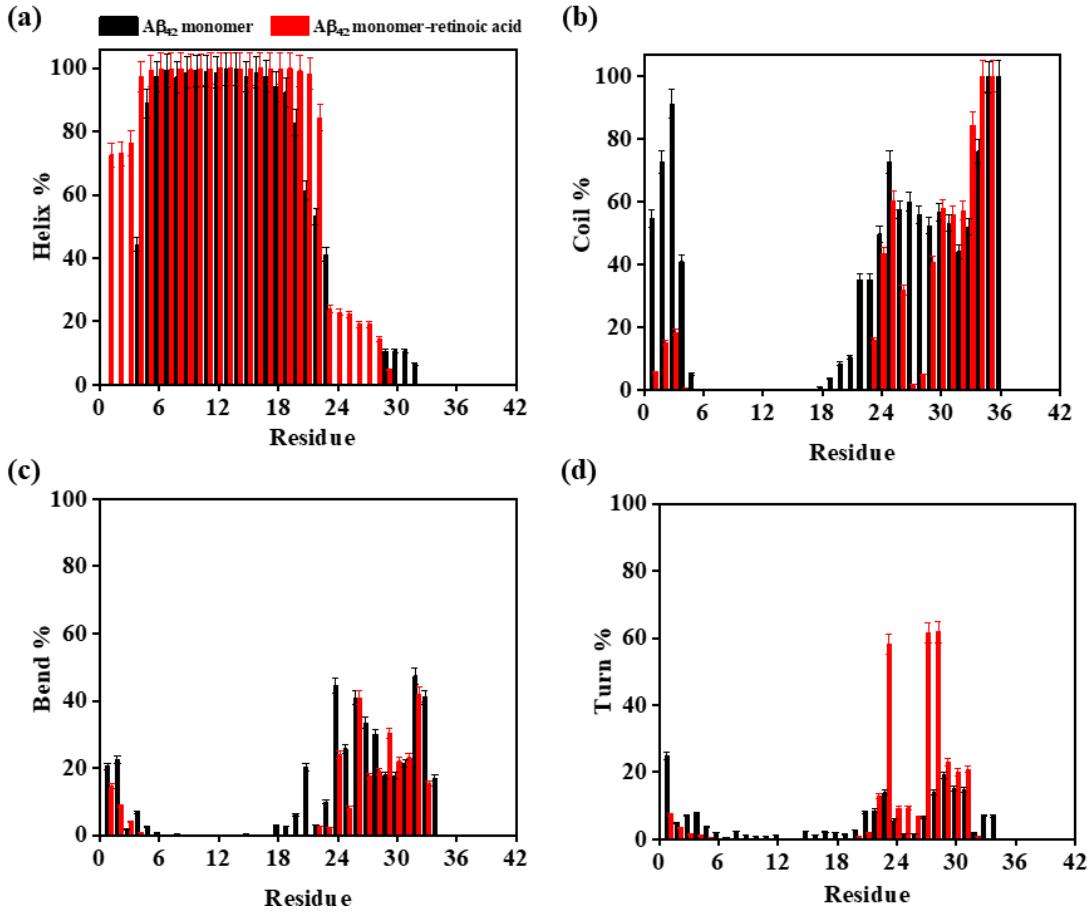

Fig. 5. Residue-wise secondary structure analysis displaying the allocation of helix (panel a); coil (panel b); bend (panel c); turn (panel d) in the simulated systems.

Furthermore, snapshots of systems were captured to compare the conformational variations in $A\beta_{42}$ monomer without and with retinoic acid (Fig. 6). A remarkable increase in helix content can be observed throughout the simulation in $A\beta_{42}$ monomer around N– and C–terminal on incorporation of retinoic acid, which matches with the secondary structure compositions (Fig. 5a). The increased helix content of $A\beta_{42}$ monomer depicts its enhanced conformational stability, on inclusion of retinoic acid.

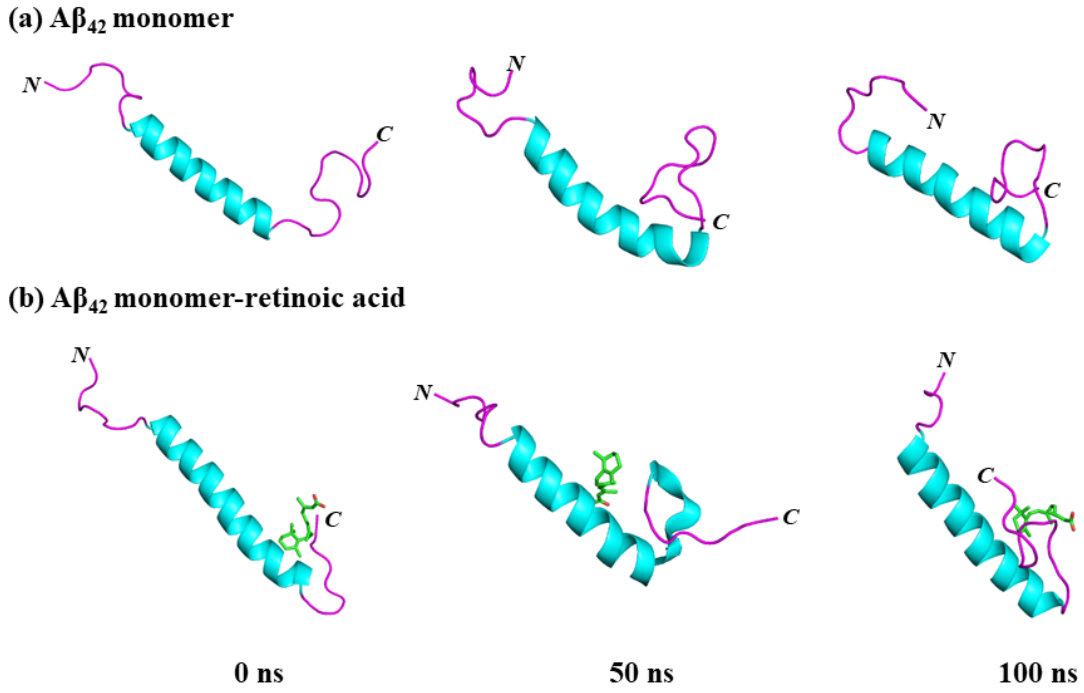

Fig. 6. Snapshots of MD trajectory at 50 ns time interval for $A\beta_{42}$ monomer (panel a) and $A\beta_{42}$ monomer-retinoic acid complex (panel b).

4.5. Effect of retinoic acid on intramolecular hydrogen bonds in $A\beta_{42}$ monomer

Intramolecular hydrogen bonding plays an important role in the investigation of the secondary structure stability of the protein in the presence of ligands.[65] The total number of intramolecular hydrogen bonds of $A\beta_{42}$ monomer, in the presence of retinoic acid, increased from 19.10 ± 0.96 to 21.07 ± 1.05 (Fig. 7). This notable increase in intramolecular hydrogen bonds indicates an increased helical conformation thereby enhancing the stability of $A\beta_{42}$ monomer.

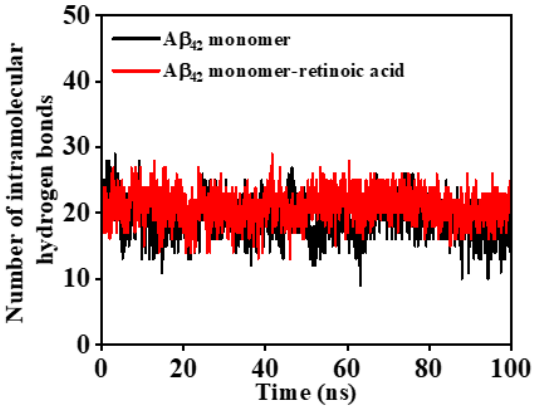

Fig. 7. Average number of intramolecular hydrogen bonds in $A\beta_{42}$ monomer and $A\beta_{42}$ monomer-retinoic acid complex.

4.6. Retinoic acid enhances conformational homogeneity in $A\beta_{42}$ monomer

Clustering analysis was employed to analyze the thermodynamic stability of $A\beta_{42}$ monomer without and with retinoic acid. The population of the most populated microstate m_1 of $A\beta_{42}$ monomer was found to be 5.25% which increased to 12.50% on the incorporation of retinoic acid (Table 6). The increase in the percentage population highlights the structural homogeneity of $A\beta_{42}$ monomer-retinoic acid complex. The population of the second and third most populated states m_2 and m_3 of $A\beta_{42}$ monomer was observed to be 3.80 and 3.50% which increased to 5.95 and 4.30% respectively, on incorporating retinoic acid. The side chain hydrogen atom of NH of Lys28 binds to the oxygen atom of carbonyl group of retinoic acid in the most populated state m_1 of $A\beta_{42}$ monomer-retinoic acid complex system (Fig. 8b). The residues of $A\beta_{42}$ monomer involved in hydrophobic contact with retinoic acid include Leu17, Ala21, Leu34, and Met35, which highlights the interaction of retinoic acid with the C–terminal and CHC–region of $A\beta_{42}$ monomer (Fig. 8c). Overall the conformational clustering analysis revealed a uniform conformational ensemble of $A\beta_{42}$ monomer with retinoic acid.

Table 6. Impact of retinoic acid on the conformational homogeneity of $A\beta_{42}$ monomer.

System	Microstates		
	m_1	m_2	m_3
$A\beta_{42}$ monomer	5.25	3.80	3.50
$A\beta_{42}$ monomer-retinoic acid	12.50	5.95	4.30

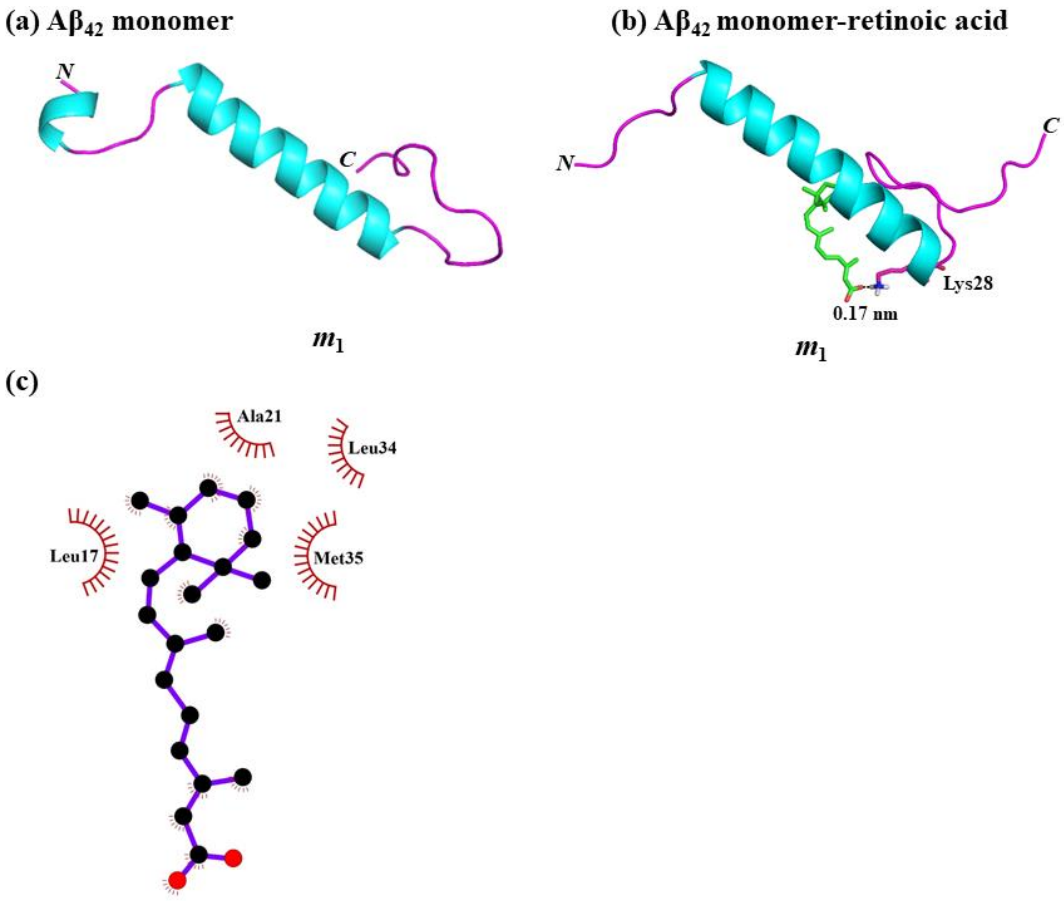

Fig. 8. Most populated state conformation (m_1) of Aβ$_{42}$ monomer (panel a); the hydrogen bond between retinoic acid and Lys28 residue of Aβ$_{42}$ peptide (panel b); 2D interaction map indicating the hydrophobic contacts in red semicircles between retinoic acid and Aβ$_{42}$ monomer (panel c).

4.7. PCA and FEL of Aβ$_{42}$ monomer and Aβ$_{42}$ monomer-retinoic acid

The 2D projection of the first two eigenvectors was used to investigate PCA and trace of the covariance matrix for Cα atoms for both Aβ$_{42}$ monomer and Aβ$_{42}$ monomer-retinoic acid complex (Fig. 9). A notable decrease in the trace value of Aβ$_{42}$ monomer from 23.35 to 10.44 nm^2 was observed on the inclusion of retinoic acid. The lower trace value illustrates the reduced conformational space of Aβ$_{42}$ monomer-retinoic acid complex, which highlights reduced conformational fluctuations of Aβ$_{42}$ monomer on the incorporation of retinoic acid.

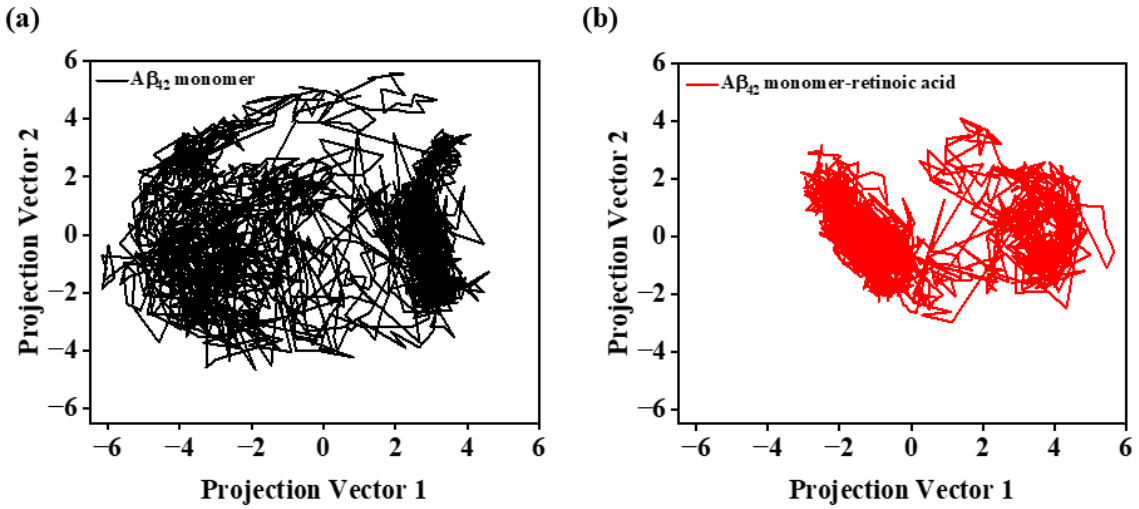

Fig. 9. Principal component analysis evaluated by 2D projection of the first two eigenvectors.

FEL was plotted using PC1 and PC2 to inspect the conformational variations of $A\beta_{42}$ monomer on the addition of retinoic acid (Fig. 10). In the absence of retinoic acid, the $A\beta_{42}$ monomer exhibited an expanded profile compared to when retinoic acid was present, which highlights increased conformational heterogeneity of $A\beta_{42}$ monomer without retinoic acid. The FEL of $A\beta_{42}$ monomer-retinoic acid complex is narrower than $A\beta_{42}$ monomer which depict conformational homogeneity of $A\beta_{42}$ monomer with retinoic acid. The FEL of $A\beta_{42}$ monomer exhibits a single minimum-energy basin with several metastable states separated by energy barriers. The FEL conformations of $A\beta_{42}$ monomer displayed 46% helix, 37% coil, 10% bend, and 7% turn (Table 7). However, $A\beta_{42}$ monomer-retinoic acid complex displayed two minimum energy conformations sampled 51–54% helix, 32–34% coil, 7% bend, and 7% turn. The results highlighted an increase in helix content in $A\beta_{42}$ monomer-retinoic acid, which matches with secondary structure results (Fig. 5a) and conformational snapshots depict stability of native helical $A\beta_{42}$ monomer in the presence of retinoic acid.

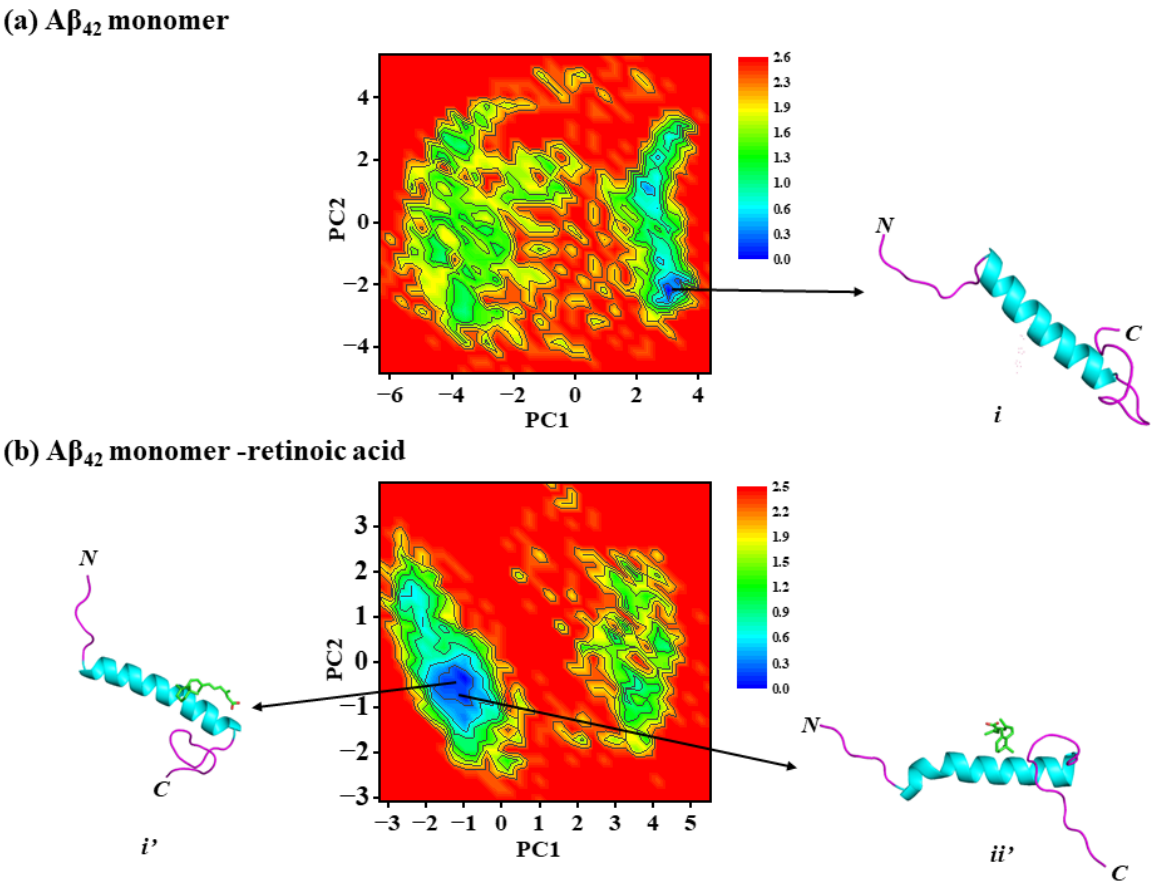

Fig. 10. Free energy landscape depicted as a function of PC1 and PC2 for the simulated systems. Minimum-energy conformations are shown in the form of cartoon representations.

Table 7. Secondary structure content of FEL conformations of simulated systems.

System	Conformation	Secondary structure component (%)				
		Helix[a]	β–sheet[b]	Coil	Bend	Turn
$A\beta_{42}$ monomer	*i*	46	0	37	10	7
$A\beta_{42}$ monomer-retinoic acid	*i'*	54	0	32	7	7
	ii''	51	0	34	7	7

[a]Helix = α–helix + π–helix + 3_{10}–helix; [b]β–sheet = β–strand + β–bridge

4.8. Calculation of binding free energy between $A\beta_{42}$ monomer and retinoic acid using MM-PBSA

The binding free energy of $A\beta_{42}$ monomer with retinoic acid was observed to be –54.89 ± 14.07 kJ mol^{-1} (Fig. 11). The van der Waals interaction was noted to be the major contributor to negative binding free energy value and displayed –62.42 ± 25.10 kJ mol^{-1}. The per residue MM-PBSA analysis depicted binding of Asp7 (–3.66 kJ mol^{-1}), Glu11 (–4.48 kJ mol^{-1}), Leu17 (–5.95 kJ mol^{-1}), Phe20 (–6.19 kJ mol^{-1}), Ala21 (–3.53 kJ mol^{-1}), Glu22 (–5.30 kJ mol^{-1}), Asp23

(–5.11 kJ mol^{-1}), Val24 (–3.09 kJ mol^{-1}), Leu34 (–4.02 kJ mol^{-1}), Met35 (– 3.67 kJ mol^{-1}), and Ala42 (–2.43 kJ mol^{-1}) with retinoic acid. Binding of Leu17, Ala21, Leu34 and Met35 residues of Aβ$_{42}$ monomer to retinoic acid is consistent with the clustering analysis (Fig. 7b). Additionally, binding of retinoic acid to CHC residues Leu17, Phe20, Ala21 of Aβ$_{42}$ monomer highlights a notable contribution in binding of retinoic acid with Aβ$_{42}$ monomer.

(a)

Energy terms	Energy (kJ mol^{-1})
	Aβ$_{42}$ monomer-retinoic acid
ΔE_{vdW}	− 62.42 ± 25.10
ΔE_{elec}	1.13 ± 0.68
ΔE_{MM} [a]	− 61.29 ± 24.42
ΔG_{ps}	14.68 ± 13.71
ΔG_{nps}	− 8.28 ± 3.36
ΔG_{solv} [b]	6.40 ± 10.35
$\Delta G_{binding}$ [c]	− 54.89 ± 14.07

[a] $\Delta E_{MM} = \Delta E_{vdW} + \Delta E_{elec}$; [b] $\Delta G_{solv} = \Delta G_{ps} + \Delta G_{nps}$; $\Delta G_{binding} = \Delta E_{MM} + \Delta G_{solv}$

(b)

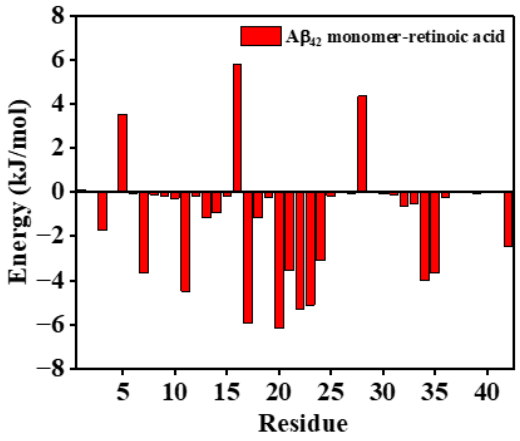

Fig. 11. Individual contributions of van der Waals, electrostatic, polar solvation, non-polar solvation in the binding free energy (panel a). Per-residue binding free energy analysis of Aβ$_{42}$ monomer-retinoic acid complex (panel b).

CHAPTER 5: Conclusion

The present study provided mechanistic insights into the vitamin A metabolite (retinoic acid)-induced modulation in $A\beta_{42}$ fibrillation. Retinoic acid displayed hydrogen bond with Val39 and hydrophobic contacts with C–terminal residues (Asn27, Ala30, Ile31, Met35, Gly38, Ile41, and Ala42) of $A\beta_{42}$ peptide. RMSD, RMSF, and SASA analyses revealed that retinoic acid lowered structural fluctuations in $A\beta_{42}$ monomer, therefore inhibiting aggregation and misfolding of Aβ peptide. Notably, retinoic acid increased the helix content of $A\beta_{42}$ monomer from 44.80 ± 2.20 to 54.40 ± 0.88%, which corroborates with higher intramolecular hydrogen bonds in $A\beta_{42}$ monomer. An increase in the helix content depicted reduced aggregation propensity of $A\beta_{42}$ monomer. The FEL highlighted increased conformational homogeneity of $A\beta_{42}$ monomer with retinoic acid. Moreover, the FEL conformations illustrated increased helical content in $A\beta_{42}$ monomer-retinoic acid, highlighting increased structural stability of $A\beta_{42}$ monomer-retinoic acid complex. Importantly, binding free energy analysis displayed favourable binding of retinoic acid in the CHC region of $A\beta_{42}$ monomer, which is consistent with the clustering analysis in which $A\beta_{42}$ monomer in m_1 displayed hydrophobic contacts of retinoic acid with the residues of CHC and C–terminal region of $A\beta_{42}$. Overall, the computational analyses unveiled inhibitory mechanism of retinoic acid against $A\beta_{42}$ fibrillation and indicated that retinoic acid prevented $A\beta_{42}$ aggregation by stabilizing the non-aggregating helical conformation of $A\beta_{42}$ monomer.

References

1. Chandel, T. I.; Zaman, M.; Khan, M.V.; Ali, M.; Rabbani, G.; Ishtikhar, M.; Khan, R.H. A mechanistic insight into protein-ligand interaction, folding, misfolding, aggregation and inhibition of protein aggregates: An overview. *Int. J. Biol. Macromol.* **2018**, *106*, 1115−1129.

2. Creighton, T.E. Protein folding. *Biochem. J.* **1990**, *270*, 1.

3. Cordes, M.H.; Davidson, A.R.; Sauer, R.T. Sequence space, folding and protein design. *Curr. Opin. Chem. Biol.* **1996**, *6*, 3–10.

4. (a) Nguyen, P.H.; Ramamoorthy, A.; Sahoo, B.R.; Zheng, J.; Faller, P.; Straub, J.E.; Dominguez, L.; Shea, J.E.; Dokholyan, N.V.; De Simone, A.; Ma, B. Amyloid oligomers: A joint experimental/computational perspective on Alzheimer's disease, Parkinson's disease, type II diabetes, and amyotrophic lateral sclerosis. *Chem. Rev*. **2021**, *121*, 2545–2647; (b) Nguyen, P.H.; Sterpone, F.; Derreumaux, P. Aggregation of disease-related peptides. *Prog. Mol. Biol. Transl. Sci.* **2020**, *170*, 435–460; (c) Iadanza, M.G.; Jackson, M.P.; Hewitt, E.W.; Ranson, N.A.; Radford, S.E. A new era for understanding amyloid structures and disease. *Nat. Rev. Mol. Cell Biol.* **2018**, *19*, 755–773.

5. (a) Soto, C.; Pritzkow, S. Protein misfolding, aggregation, and conformational strains in neurodegenerative diseases. *Nat. Neurosci.* **2018**, *21*, 1332–1340; (b) Chiti, F.; Dobson, C.M. Protein misfolding, amyloid formation, and human disease: a summary of progress over the last decade. *Annu. Rev. Biochem.* **2017**, *86*, 27–68.

6. https://www.alzint.org/about/dementia-facts-figures/

7. (a) Hippius H.; Neundörfer G. The discovery of Alzheimer's disease. *Dialogues Clin. Neurosci*. **2003**, *5*, 101−108; (b) Alzheimer A. Über Eine Eigenartige Erkrankung Der Hirnrinde. Allg. Zschr. Psychiat. *Psych. gerichtl. Med*. **1907**, *64*, 146−148.

8. Goedert M.; Spillantini M. G. A century of Alzheimer's disease. *Science* **2006**, *314*, 777−781.

9. (a) Ono K. Alzheimer's disease as oligomeropathy. *Neurochem. Int.* **2018**, *119*, 57–70; (b) Murphy P. M.; LeVine H. Alzheimer's disease and the amyloid-β peptide. *J. Alzheimer's Dis.* **2010**, *19*, 311–323.

10. (a) Sierra-Fonseca, J.A.; Gosselink, K.L. Tauopathy and neurodegeneration: a role for stress. *Neurobiol. Stress* **2018**, *9*, 105−112; (b) Šimić, G.; Babić Leko, M.; Wray, S., Harrington; C., Delalle, I.; Jovanov-Milošević, N.; Bažadona, D.; Buée, L.; De Silva, R.; Di Giovanni, G.; Wischik, C. Tau protein hyperphosphorylation and aggregation in Alzheimer's disease and other tauopathies, and possible neuroprotective strategies. *Biomolecules* **2016**, *6*, 6; (c) Nisbet, R.M.; Polanco, J.C.; Ittner, L.M.; Götz, J. Tau aggregation and its interplay with amyloid-β. *Acta. Neuropathol.* **2015**, *129*, 207–220.

11. Selkoe, D.J. Translating cell biology into therapeutic advances in Alzheimer's disease. *Nature* **1999**, *399*, A23-A31.

12. (a) Hamley, I.W. The amyloid beta peptide: a chemist's perspective. Role in Alzheimer's and fibrillization. *Chem. Rev.* **2012**, *112*, 5147–5192. (b) Mattson, M.P. Cellular actions of beta-amyloid precursor protein and its soluble and fibrillogenic derivatives. *Physiol. Rev.* **1997**, *77*, 1081–1132.

13. (a) Xi, W.; Vanderford, E.K.; Hansmann, U.H. Out-of-register $A\beta_{42}$ assemblies as models for neurotoxic oligomers and fibrils. *J. Chem. Theory Comput.* **2018** *14*, 1099–1110. (b) Xi, W.; Hansmann, U.H. Ring-like N-fold Models of $A\beta_{42}$ fibrils. *Sci. Rep.* **2017**, *7*, 6588. (c) Ahmed, M.; Davis, J.; Aucoin, D.; Sato, T.; Ahuja, S.; Aimoto, S.; Elliot, J. I.; Van Nostrand. W. E.; Smith, S. O. Structural conversion of neurotoxic amyloid−β_{1-42} oligomers to fibrils. *Nat. Struc. Mol. Biol.* **2010**, *17*, 561−567.

14. Stefani, M.; Dobson, C.M. Protein aggregation and aggregate toxicity: New insights into protein folding, misfolding diseases and biological evolution. *J. Mol. Med.* **2003**, *81*, 678 –699.

15. (a) Mishra, C.B.; Shalini, S.; Gusain, S.; Kumar, P.; Kumari, S.; Choi, Y.S.; Kumari, J.; Moku, B.K.; Yadav, A.K.; Prakash, A.; Jeon, R. Multitarget action of benzothiazole-piperazine small hybrid molecule against Alzheimer's disease: *In silico*, *in vitro*, and *in vivo* investigation. *Biomed. Pharmacother.* **2024**, *174*, 116484. (b) Nam, Y.; Prajapati, R.; Kim, S.; Shin, S.J.; Park, Y.H.; Park, H.H.; Lim, D.; Yoon, Y.; Lee, G.; Jung, H.A.; Park, I. Dual regulatory effects of neferine on amyloid-β and tau aggregation studied by *in silico*, *in vitro*, and lab-on-a-chip technology. *Biomed. Pharmacother.* **2024**, *172*, 116226 (c) Hadidi, S.; Farzaei, M.H. Inhibitory activity of natural flavonoids against protein aggregation in Alzheimer's disease: A computational simulation study. *Adv J Chem Sect A* **2023**, *6*, 123−140. (d) Chen, X.; Li, Y.; Kang, J.; Ye, T.; Yang, Z.; Liu, Z.; Liu, Q.; Zhao, Y.; Liu, G.; Pan, J. Application of a novel coumarin-derivative near-infrared fluorescence probe to amyloid-β imaging and inhibition in Alzheimer's disease. *J. Lumin.* **2023**, *256*, 119661. (e) Wang, X.X.; Xie, F.; Jia, C.C.; Yan, N.; Zeng, Y.L.; Wu, J.D.; Liu, Z.P. Synthesis and biological evaluation of selective histone deacetylase 6 inhibitors as multifunctional agents against Alzheimer's disease. *Eur. J. Med. Chem.* **2021**, *225*, 113821.

16. (a) Kaur, B.; Kaur, R.; Vivesh, Rani, S.; Bhatti, R.; Singh, P. Small Peptides Targeting BACE-1, AChE, and A-β reversing scopolamine-induced memory impairment: A multitarget approach against Alzheimer's disease. *ACS Omega* **2024**, *9*, 12896−12913. (b) Mallesh, R.; Juhee khan; Gharai, P.K.; Gupta, V.; Roy, R.; Ghosh, S. Controlling Amyloid beta peptide aggregation and toxicity by protease-stable ligands. *ACS Bio. Med. Chem. Au.* **2023**, *3*, 158−173. (c) Kundal, K.; Paramasivam, S.; Mitra, A.; Sarkar, N. *In silico* identification of novel peptides as potential modulators of Aβ42 amyloidogenesis. *BioRxiv* **2022**, 2022−2049. (d) Consoli, G.M.L.; Tosto, R.; Baglieri, A.; Petralia, S.; Campagna, T.; Di Natale, G.; Zimbone, S.; Giuffrida, M.L.; Pappalardo, G. Novel peptide-calix [4] arene conjugate inhibits Aβ aggregation and rescues neurons from Aβ's oligomers cytotoxicity *in vitro*. *ACS Chem. Neurosci.* **2021**, *12*, 1449−1462. (e) Jokar, S.; Erfani, M.; Bavi, O.; Khazaei, S.; Sharifzadeh, M.; Hajiramezanali, M.; Beiki, D.; Shamloo, A. Design of peptide-based inhibitor agent against amyloid-β aggregation: Molecular docking, synthesis and *in vitro* evaluation. *Bioorg. Chem.* **2020**, *102*, 104050.

17. (a) Mani, R.; Ezhumalai, D.; Muthusamy, G.; Namasivayam, E. Neuroprotective effect of biogenically synthesized ZnO nanoparticles against oxidative stress and β-amyloid

toxicity in transgenic *Caenorhabditis elegans Appl. Biochem. Biotechnol*. **2024**, *71*, 132−146. (b) Nguyen, N.K.; Poduska, B.; Franks, M.; Bera, M.; MacCormack, I.; Lin, G.; Petroff, A.P.; Das, S.; Nag, A. A copper-selective sensor and its inhibition of copper-amyloid beta aggregation. *Biosensors* **2024**, *14*, 247. (c) Eremina, O.E.; Yarenkov, N.R.; Bikbaeva, G.I.; Kapitanova, O.O.; Samodelova, M.V.; Shekhovtsova, T.N.; Kolesnikov, I.E.; Syuy, A.V.; Arsenin, A.V.; Volkov, V.S.; Tselikov, G.I. Silver nanoparticle-based SERS sensors for sensitive detection of amyloid-β aggregates in biological fluids. *Talanta* **2024**, *266*, 124970. (d) Saleh, S.R.; Abd-Elmegied, A.; Madhy, S.A.; Khattab, S.N.; Sheta, E.; Elnozahy, F.Y.; Mehanna, R.A. Ghareeb, D.A.; Abd-Elmonem, N.M. Brain-targeted Tet-1 peptide-PLGA nanoparticles for berberine delivery against STZ-induced Alzheimer's disease in a rat model: Alleviation of hippocampal synaptic dysfunction, Tau pathology, and amyloidogenesis. *Int. J. Pharm.* **2024**, *658*, 124218. (e) Far, B.F., Safaei, M., Pourmolaei, A., Adibamini, S., Shirdel, S., Shirdel, S., Emadi, R. and Kaushik, A.K., Exploring curcumin-loaded lipid-based nanomedicine as efficient targeted therapy for Alzheimer's diseases. *ACS Appl. Bio Mater*. **2024**, *7*, 3535–3555.

18. Dash, P.K.; Moore, A.N.; Orsi, S.A. Blockade of γ-secretase activity within the hippocampus enhances long-term memory. *Biochem. Biophys. Res. Commun*. **2005**, *338*, 777−782.

19. (a) Asai, M.; Hattori, C.; Iwata, N.; Saido, T.C.; Sasagawa, N.; Szabó, B.; Hashimoto, Y.; Maruyama, K.; Tanuma, S.I.; Kiso, Y.; Ishiura, S. The novel β-secretase inhibitor KMI-429 reduces amyloid β peptide production in amyloid precursor protein transgenic and wild-type mice. *J. Neurochem*. **2006**, *96*, 533− 540. (b) Bacskai, B.J.; Kajdasz, S.T.; Christie, R.H.; Carter, C.; Games, D.; Seubert, P.; Schenk, D.; Hyman, B.T. Imaging of amyloid-β deposits in brains of living mice permits direct observation of clearance of plaques with immunotherapy. *Nat. Med*. **2001**, *7*, 369−372.

20. Doig, A.J.; Derreumaux, P. Inhibition of protein aggregation and amyloid formation by small molecules. *Curr. Opin. Struct. Biol*. **2015**, *30*, 50−56.

21. Tayeb, H.O.; Yang, H.D.; Price, B.H.; Tarazi, F.I. Pharmacotherapies for Alzheimer's disease: Beyond cholinesterase inhibitors. *Pharmacol. Ther.* **2012**, *134*, 8−25.

22. (a) Lee, V.; Rekhi, E.; Kam, J.H.; Jeffery, G. Vitamin D rejuvenates aging eyes by reducing inflammation, clearing amyloid beta and improving visual function. *Neurobiol. Aging* **2012**, *33*, 2382–2389. (b) Annweiler, C.; Brugg, B.; Peyrin, J.M.; Bartha, R.; Beauchet, O. Combination of memantine and vitamin D prevents axon degeneration induced by amyloid-beta and glutamate. *Neurobiol. Aging* **2014**, *35*, 331−335.

23. Huy, P.D.Q.; Yu, Y.C.; Ngo, S.T.; Van Thao, T.; Chen, C.P.; Li, M.S.; Chen, Y.C. *In silico* and *in vitro* characterization of anti-amyloidogenic activity of vitamin K3 analogues for Alzheimer's disease. *Biochim. Biophys. Acta -Gen. Subj.* **2013**, *1830*, 2960−2969.

24. Murakami, K.; Murata, N.; Ozawa, Y.; Kinoshita, N.; Irie, K.; Shirasawa, T.; Shimizu, T. Vitamin C restores behavioral deficits and amyloid-β oligomerization without affecting plaque formation in a mouse model of Alzheimer's disease. *J. Alzheimer's Dis*. **2011**, *26*, 7−18.

25. Andrade, S.; Loureiro, J.A.; Pereira, M.C. Vitamin B12 inhibits Aβ fibrillation and disaggregates preformed fibrils in the presence of synthetic neuronal membranes. *ACS Chem. Neurosci.* **2021**, *12*, 2491−2502.

26. Joshi, P.; Chia, S.; Yang, X.; Perni, M.; Gabriel, J.M.; Gilmer, M.; Limbocker, R.; Habchi, J.; Vendruscolo, M. Combinations of Vitamin A and Vitamin E metabolites confer resilience against Amyloid-β aggregation. *ACS Chem. Neurosci.* **2023**, *14*, 657−666.

27. Qais, F.A.; Parveen, N.; Afzal, M.; Furkan, M.; Khan, R.H. Preventing amyloid-β oligomerization and aggregation with berberine: Investigating the mechanism of action through computational methods. *Int. J. Biol. Macromol.* **2024**, *258*, 128900.

28. Zakaria, N.; Harun, W.M.R.S.W.; Latif, M.A.M., Azaman; S.N.A., Rahman, M.B.A.; Faujan, N.H. Effects of anthocyanidins on the conformational transition of Aβ (1−42) peptide: Insights from molecular docking and molecular dynamics simulations. *J. Mol. Graph.* **2024**, *129*, 108732.

29. Mishra, C.B.; Shalini, S.; Gusain, S.; Kumar, P.; Kumari, S.; Choi, Y.S.; Kumari, J.; Moku, B.K.; Yadav, A.K.; Prakash, A.; Jeon, R. Multitarget action of benzothiazole-piperazine small hybrid molecule against Alzheimer's disease: *In silico*, *in vitro*, and *in vivo* investigation. *Biomed. Pharmacother.* **2024**, *174*, 116484.

30. Nam, Y.; Prajapati, R.; Kim, S.; Shin, S.J.; Park, Y.H.; Park, H.H.; Lim, D.; Yoon, Y.; Lee, G.; Jung, H.A.; Park, I. Dual regulatory effects of neferine on amyloid-β and tau aggregation studied by *in silico*, *in vitro*, and lab-on-a-chip technology. *Biomed. Pharmacother.* **2024**, *172*, 116226.

31. Firouzi, R.; Sowlati-Hashjin, S.; Chávez-García, C.; Ashouri, M.; Karimi-Jafari, M.H.; Karttunen, M. Identification of catechins' binding sites in monomeric Aβ42 through ensemble docking and MD simulations. *Int. J. Mol. Sci.* **2023**, *24*, 8161.

32. Baruah, P.; Moorthy, H.; Ramesh, M.; Padhi, D.; Govindaraju, T. A natural polyphenol activates and enhances GPX4 to mitigate amyloid-β induced ferroptosis in Alzheimer's disease. *Chem. Sci.* **2023**, *14*, 9427−9438.

33. Radwan, A.; Alanazi, F. Combined modeling study of the binding characteristics of natural compounds, derived from Psoralea fruits, to β-amyloid peptide monomer. *Int. J. Mol. Sci.* **2022**, *23*, 3546.

34. Fang, M.; Zhang, Q.; Wang, X.; Su, K.; Guan, P.; and Hu, X. Inhibition mechanisms of (−)-epigallocatechin-3-gallate and genistein on Amyloid-beta 42 peptide of Alzheimer's disease via molecular simulations. *ACS Omega* **2022**, *7*, 19665−19675.

35. Pasieka, A.; Panek, D.; Szałaj, N.; Espargaró, A.; Więckowska, A.; Malawska, B.; Sabaté, R.; Bajda, M. Dual inhibitors of amyloid-β and tau aggregation with amyloid-β disaggregating properties: extended *in cellulo*, *in silico*, and kinetic studies of multifunctional anti-Alzheimer's agents. *ACS Chem. Neurosci.* **2021**, *12*, 2057−2068.

36. González-Sanmiguel, J.; Burgos, C.F.; Bascuñán, D.; Fernández-Pérez, E.J.; Riffo-Lepe, N.; Boopathi, S.; Fernández-Pérez, A.; Bobadilla-Azócar, C.; González, W.; Figueroa, M.;

Vicente, B. Gabapentin inhibits multiple steps in the amyloid beta toxicity cascade. *ACS Chem. Neurosci.* **2020**, *11*, 3064−3076.

37. Peters, C.; Bascuñán, D.; Burgos, C.F.; Bobadilla, C.; González-Sanmiguel, J.; Boopathi, S.; Riffo, N.; Fernández-Pérez, E.J.; Tarnok, M.E.; Aguilar, L.F.; Gonzalez, W. Characterization of a new molecule capable of inhibiting several steps of the amyloid cascade in Alzheimer's disease. *Neurobiol. Dis.* **2020**, *141*, 104938.

38. Mallesh, R.; Juhee khan; Gharai, P.K.; Gupta, V.; Roy, R.; Ghosh, S. Controlling amyloid beta peptide aggregation and toxicity by protease-stable ligands. *ACS Bio. Med. Chem. Au.* **2023**, *3*, 158−173.

39. Kundal, K.; Paramasivam, S.; Mitra, A.; Sarkar, N. *In silico* identification of novel peptides as potential modulators of Aβ42 amyloidogenesis. *BioRxiv* **2022**, 2022−2049.

40. Konar, M.; Ghosh, D.; Samanta, S.; Govindaraju, T. Combating amyloid-induced cellular toxicity and stiffness by designer peptidomimetics. *RSC Chem. Biol.* **2022**, *3*, 220−226.

41. Liu, W.; Sun, X.; Dong, X.; Sun, Y. Chiral LVFFARK enantioselectively inhibits amyloid-β protein fibrillogenesis. *Chin. J. Chem. Eng*. **2022**, *48*, 227−235.

42. Tomaselli S.; Esposito V.; Vangone P.; van Nuland NA.; Bonvin AM.; Guerrini R.; Tancredi T.; Temussi PA.; Picone D. The alpha-to-beta conformational transition of Alzheimer's Abeta− (1− 42) peptide in aqueous media is reversible: A step by step conformational analysis suggests the location of beta conformation seeding. *Chem. Biochem.* **2006**, *7*, 257−67.

43. Zardecki, C.; Dutta, S.; Voigt, M.; Burley, S. K. RCSB Protein data bank: A resource for chemical, biochemical, and structural exploration of large and small biomolecules. *J. Chem. Educ.* **2016**, 93, 569−575.

44. Mills, N. ChemDraw Ultra 10.0. *J. Am. Chem. Soc.* **2006**, *128*, 13649−13650

45. Frisch, M. J.; Trucks, G. W.; Schlegel, H. B.; Scuseria, G. E.; Robb, M. A.; Cheeseman, J. R.; Scalmani, G.; Barone, V.; Petersson, G. A.; Nakatsuji, H.; Li, X.; Caricato, M.; Marenich, A.; Bloino, J.; Janesko, B. G.; Gomperts, R.; Mennucci, B.; Hratchian, H. P.; Ortiz, J. V.; Izmaylov, A. F.; Sonnenberg, J. L.; Williams-Young, D.; Ding, F.; Lipparini, F.; Egidi, F.; Goings, J.; Peng, B.; Petrone, A.; Henderson, T.; Ranasinghe, D.; Zakrzewski, V. G.; Gao, J.; Rega, N.; Zheng, G.; Liang, W.; Hada, M.; Ehara, M.; Toyota, K.; Fukuda, R.; Hasegawa, J.; Ishida, M.; Nakajima, T.; Honda, Y.; Kitao, O.; Nakai, H. Vreven, T.; Throssell, K.; Montgomery, Jr.; Peralta, J. E.; Ogliaro, F.; Bearpark, M.; Heyd, J. J.; Brothers, E.; Kudin, K.N.; Staroverov, V.N.; Keith, T.; Kobayashi, R.; Normand, J.; Raghavachari, K.; Rendell, A.; Burant, J.C.; Iyengar, S. S.; Tomasi, J.; Cossi, M.; Millam, J. M.; Klene, M.; Adamo, C.; Cammi, R.; Ochterski, J. W.; Martin, R. L.; Morokuma, K.; Farkas O., Foresman, J. B.; Fox, D. J. Gaussian 09, Revision A.02. *Gaussian, Inc., Wallingford CT*, **2016**.

46. Malde K. A.; Zuo L.; Breeze M.; Stroet M.; Poger D.; Nair C. P.; Oostenbrink C.; E. A. Mark. An Automated Force Field Topology Builder (ATB) and repository: Version 1.0. *J. Chem. Theory Comput.* **2011**, *7*, 4026−4037.

47. Best R.B.; Zhu X.; Shim J.; Lopes P.E.M.; Mittal J.; Feig M.; MacKerell Jr. A.D. "Optimization of the additive CHARMM all-atom protein force field targeting improved sampling of the backbone phi, psi and side-chain chi1 and chi2 dihedral angles," *J. Chem. Theory Comput.* **2012**, *8*, 3257−3273.

48. Trott O.; Olson A. J. AutoDock Vina: Improving the speed and accuracy of docking with a new scoring function, efficient optimization and multithreading. *J. Comput. Chem.* **2010**, *31*, 455−461.

49. Morris, G. M.; Goodsell, D. S.; Halliday, R.S.; Huey, R.; Hart, W. E.; Belew, R.K.; Olson, A. J. Automated docking using Lamarckian genetic algorithm and an empirical binding free energy function. *J. Comput. Chem.* **1998**, *19*, 1639−1662.

50. Huey R.; Morris G. M.; Olson A. J.; Goodsell D. S.; A semiempirical free energy force field with charge-based desolvation. *J. Comput. Chem.* **2007**, *28*, 1145−1152;

51. Solis J. F.; Wets J.-B. R. Minimization by random search techniques. *Math. Oper. Res.* **1981**, *6*, 19−30.

52. Laskowski R. A.; Swindells M. B. LigPlot+: Multiple ligand-protein interaction diagrams for drug discovery. *J. Chem. Inf. Model.*, **2011**, *51*, 2778−2786;

53. DeLano W. L. The PyMOL molecular graphics system. **2002**, *571*, DeLano Scientific, San Carlos, CA.

54. (a) Abraham M. J.; Murtola T.; Schulz R.; Pall S.; Smith J. C.; Hess B.; E. Lindahl. GROMACS: High performance molecular simulations through multi-level parallelism from laptops to supercomputers. *SoftwareX* **2015**, *1*, 19−25; (b) Van Der Spoel D.; Lindahl E.; Hess B.; Groenhof G.; Mark A. E.; Berendsen H. J. C. GROMACS: Fast, flexible, and free. *J. Comput. Chem.* **2005**, *26*, 1701−1718.

55. Mark, P.; Nilsson, L. Structure and dynamics of the TIP3P, SPC, and SPC/E water models at 298 K. *J. Phys. Chem. A.* **2001**, *10*, 9954−9960.

56. Bussi G.; Donadio D.; Parrinello M. Canonical sampling through velocity rescaling. *J. Chem. Phys.* **2007**, *126*, 014101.

57. Parrinello M.; Rahman A. Polymorphic transitions in single crystals: A new molecular dynamics method. *J. Appl. Phys*. **1981**, *52*, 7182–7190.

58. Hess B.; Bekker H.; Berendsen H. J. C.; Fraaije J. G. E. M.; LINCS: A linear constraint solver for molecular simulations. *J. Comput. Chem.*, **1997**, *18*, 1463−1472.

59. (a) Essmann U.; Perera L.; Berkowitz M. L.; Darden T.; Lee H.; Pedersen L. G. A smooth particle mesh Ewald method. *J. Chem. Phys.*, **1995**, *103*, 8577−8593; (b) Darden T.; York D.; Pedersen L. Particle mesh Ewald: An $N\cdot\log(N)$ method for Ewald sums in large systems. *J. Chem. Phys.* **1993**, *98*, 10089−10092.

60. Kabsch W.; Sander C. Dictionary of protein secondary structure: Pattern recognition of hydrogen-bonded and geometrical features. *Biopolymers* **1983**, *22*, 2577−2637.

61. (a) Smith L. J.; Daura X.; van Gunsteren W. F.Assessing equilibration and convergence in biomolecular simulations. *Proteins: Struct. Funct. Genet.* **2002**, *48*, 487-96; (b) Daura X.; Gademann K.; Jaun B.; Seebach D.; van Gunsteren W. F., Mark A. E. Peptide folding: When simulation meets experiment. *Angew. Chem. Int. Ed.* **1999**, *38*, 236−240.

62. (a) Genheden S.; Ryde U. The MM/PBSA and MM/GBSA methods to estimate ligand binding affinities. *Expert Opin. Drug Discov.* **2015**, *10*, 449−461. (b) Kumari, R; Kumar R. g_mmpbsa-A GROMACS tool for high-throughput MM-PBSA calculations. *J. Chem. Inf. Model.* **2014**, *54*, 1951−1962.

63. Peters, C.; Bascuñán, D.; Burgos, C.F.; Bobadilla, C.; González-Sanmiguel, J.; Boopathi, S.; Riffo, N.; Fernández-Pérez, E.J.; Tarnok, M.E.; Aguilar, L.F.; Gonzalez, W. Characterization of a new molecule capable of inhibiting several steps of the amyloid cascade in Alzheimer's disease. *Neurobiol. Dis.* **2020**, *141*, 104938.

64. (a) Bertini, I.; Gonnelli, L.; Luchinat, C.; Mao, J.; Nesi, A. A new structural model of Aβ40 fibrils. *J. Am. Chem. Soc.* **2011** *133*, 16013–16022; (b) Tjernberg, L.O.; Lilliehöök, C.; Callaway, D.J.; Näslund, J.; Hahne, S.; Thyberg, J.; Terenius, L.; Nordstedt, C. Controlling amyloid β-peptide fibril formation with protease-stable ligands. *J. Biol. Chem*. **1997**, *272*, 12601–12605; (c) Li, H., Rahimi, F. and Bitan, G., Modulation of amyloid β-protein (Aβ) assembly by homologous C-terminal fragments as a strategy for inhibiting Aβ toxicity. *ACS Chem. Neurosci*. **2016**, *7*, 845–856.

65. Newberry, R.W.; Raines, R.T. Secondary forces in protein folding. *ACS Chem. Biol.* **2019,** *14*, 1677−1686.

msc-vg-revised

ORIGINALITY REPORT

16%	8%	16%	0%
SIMILARITY INDEX	INTERNET SOURCES	PUBLICATIONS	STUDENT PAPERS

PRIMARY SOURCES

1	Apneet Kaur, Bhupesh Goyal. "Identification of new pentapeptides as potential inhibitors of amyloid–β42 aggregation using virtual screening and molecular dynamics simulations", Journal of Molecular Graphics and Modelling, 2023 Publication	3%
2	Kamaljot Singh, Anupamjeet Kaur, Deepti Goyal, Bhupesh Goyal. "Mechanistic insights into the mitigation of Aβ aggregation and protofibril destabilization by a D–enantiomeric decapeptide rk10", Physical Chemistry Chemical Physics, 2022 Publication	2%
3	Rajneet Kaur Saini, Suniba Shuaib, Deepti Goyal, Bhupesh Goyal. " Insights into the inhibitory mechanism of a resveratrol and clioquinol hybrid against Aβ aggregation and protofibril destabilization: A molecular dynamics simulation study ", Journal of Biomolecular Structure and Dynamics, 2018 Publication	1%

Vibhuti

Bhupesh Goyal
30/7/2024